Energy-conserving methods for the nonlinear Schroedinger equation

Energy-conserving methods for the nonlinear Schrödinger equation

L. Barletti[a], L. Brugnano[a], G. Frasca Caccia[b], F. Iavernaro[c]

[a] *Dipartimento di Matematica e Informatica "U. Dini", Università di Firenze, Firenze, Italy*
[b] *School of Mathematics, Statistics & Actuarial Science, University of Kent, Canterbury, UK*
[c] *Dipartimento di Matematica, Università di Bari, Bari, Italy*

Abstract

In this paper, we further develop recent results in the numerical solution of Hamiltonian partial differential equations (PDEs) [14], by means of energy-conserving methods in the class of Line Integral Methods, in particular, the Runge-Kutta methods named Hamiltonian Boundary Value Methods (HBVMs). We shall use HBVMs for solving the nonlinear Schrödinger equation (NLSE), of interest in many applications. We show that the use of energy-conserving methods, able to conserve a discrete counterpart of the Hamiltonian functional, confers more robustness on the numerical solution of such a problem.

Keywords: Hamiltonian partial differential equations, nonlinear Schrödinger equation, energy-conserving methods, line integral methods, Hamiltonian Boundary Value methods, HBVMs.

2010 MSC: 65P10, 65M20, 65L05

1. Introduction

In this paper we discuss energy-conservation issues when numerically solving the following general form of nonlinear Schrödinger equation (NLSE),

$$i\psi_t(x,t) + \psi_{xx}(x,t) + f'(|\psi(x,t)|^2)\psi(x,t) = 0, \quad (x,t) \in \Omega = [a,b] \times [0,T],$$
(1)

with i the imaginary unit and f' the derivative of f, coupled with suitable initial data, and periodic boundary conditions.

The interest around the NLSE has been progressively growing in the last half century. Starting from its first appearance as a mathematical model to describe laser beams [33], the possible applications of the NLSE has widened to include several important areas of research. Roughly speaking, the NLSE can arise as the first-order approximation of Maxwell equations in a nonlinear medium, or as the mean-field approximation of a many-body quantum problem. In the first case it finds applications to fiber optics communications [2], plasma physics [53], geophysics [52] and mathematical biology [51]. In the second case, it is largely employed in quantum chemistry and condensed matter physics. In low-temperature physics, in particular, it is worth to mention the fact that a Bose-Einstein condensate behaves like a "giant wavefunction", which can be described by means of a suitable version of the NLSE, known as the Gross-Pitaevskii equation [34, 54].

The reason for such ubiquity of the NLSE is partially explained by its conservation properties and Galilean invariance [29]. Moreover, it can be shown that the NLSE is always found as the first-order in the perturbative expansion of a large class of dispersive nonlinear equations [35].

From the strictly mathematical point of view, the one-dimensional cubic NLSE has gained great attention since 1972, when Zakharov and Shabat [62] were able to exhibit a Lax pair for such NLSE, thus proving that it is a completely integrable PDE. This implies that the NLSE can be studied with the methods of Inverse Scattering Transform (IST) [1]. Very recently, it has even been proposed that IST could provide a method of encoding an information to be optically transmitted, putting somehow the NLSE at the basis of a possible technological revolution [43, 61].

Because of its many applications and interesting features, the numerical study of the NLSE is of considerable interest and many numerical methods have been investigated for its solution. Different approaches have been considered by different authors in the last decades.

Finite-difference and finite-element schemes preserving discrete analogue of energy and momentum of (1) with a polynomial nonlinearity have been developed in [36, 55, 57].

A completely different approach is at the basis of multisymplectic integrators, defined by Bridges and Reich [7] as discretizations preserving a discrete conservation of symplecticity of a general form

$$\delta_t \omega_i^n + \delta_x^+ \kappa_i^n,$$

where δ_t and δ_x represent the (abstract) time and space discretization oper-

ators respectively and ω_i^n and κ_i^n are discrete forms [8, 49]. Applications of several multisymplectic schemes to the nonlinear Schrödinger equation can be found, e.g., in [30, 31, 32, 45, 46, 47, 48].

A different strategy is to use a method of lines approach, where one first sets a spatial discretization of (1) (usually by means of a Fourier spectral method [38, 39] or by a finite difference method [3, 40, 60]) providing a Hamiltonian system of ODEs. Then, for the full discretization in time the most convenient strategy is to use a symplectic method [7, 32, 44, 56, 58, 59], or an energy conserving method.

Symplectic methods are able to produce accurate results and to preserve very well the energy of the original system over long times [58, 6, 42]. In particular, one can consider splitting methods [3, 37, 38, 39, 40, 50, 60], whose leading idea is to solve the given system of ODEs by means of a sequence of steps in which alternatively the dispersive or the nonlinear term is set to zero. Splitting methods have the advantage to provide symplectic and explicit schemes. On the other hand, the understanding of the long-time behaviour of splitting methods for Hamiltonian PDEs is a fundamental ongoing challenge in the field of geometric integration and they are usually subject to CFL conditions, imposing some constraint on the stepsize in time depending on the parameters used in the spatial discretization [3, 38]. In [39] the authors use a modulated Fourier expansion to investigate the approximate conservation over long times of energy and momentum of (1) with a cubic nonlinearity, when a Fourier method is used in space and a Lie-Trotter or a Strang splitting is used for the full discretization.

Differently, one can choose to use an energy-conserving method in time for solving the Hamiltonian system of ODEs provided after the discretization in space as done in [12, 13, 14] or in [41] for a NLSE equation including a wave operator.

The latter is the strategy we are going to adopt in this paper. More specifically, after a Fourier-Galerkin space semi-discretization, we employ a method in the class of HBVMs (see, e.g., the recent monographh [16]) to get the full discretized problem, thus extending to the NLSE the approach used in [14] for the semi-linear wave equation (see also [5], where some preliminary results are given).

With these premises, in Section 2 we state the main facts about the NLSE and its space semi-discretization. Then, in Section 3 we sketch the main properties of the energy-conserving Runge-Kutta schemes known as HBVMs. The efficient implementation of the methods, when numerically

3

solving (1) is studied in Section 4. Some numerical tests are reported in Section 5 and, finally, some concluding remarks are given in Section 6.

2. Properties and space semi-discretization

Equation (1) can be rewritten in real form by setting

$$\psi(x,t) = u(x,t) + iv(x,t), \tag{2}$$

with u and v the real and imaginary part of ψ, respectively. In so doing, one obtains:[1]

$$
\begin{aligned}
u_t &= -v_{xx} - f'(u^2 + v^2)v, \\
v_t &= u_{xx} + f'(u^2 + v^2)u, \qquad (x,t) \in \Omega,
\end{aligned}
\tag{3}
$$

or, more compactly, by setting

$$y = \begin{pmatrix} u \\ v \end{pmatrix}, \qquad J = \begin{pmatrix} 0 & 1 \\ -1 & 0 \end{pmatrix} \equiv -J^\top \equiv -J^{-1},$$

as

$$y_t = J\nabla\mathcal{H}[y], \tag{4}$$

with $\nabla\mathcal{H}[y]$ the vector with the *functional derivatives*, w.r.t. u and v, of the *Hamiltonian functional*

$$\mathcal{H}[y] \equiv \mathcal{H}[u,v] = \frac{1}{2} \int_a^b \left(u_x^2 + v_x^2 - f(u^2 + v^2) \right) \mathrm{d}x. \tag{5}$$

Such functional defines the equation which is, therefore, an instance of *Hamiltonian PDE*. Because of the periodic boundary conditions, the following result holds true.

Theorem 1. *Under regularity assumptions on f and on the initial data, the Hamiltonian functional (5) is constant along the solution of (3).*

---

[1]For sake of brevity, we shall omit the arguments of u and v, when unnecessary.

<u>Proof</u>   In fact, from (5) and (3), one obtains[2]

$$
\begin{aligned}
\dot{\mathcal{H}}[u,v] &= \int_a^b \left(u_x u_{xt} + v_x v_{xt} - f'(u^2+v^2)(uu_t+vv_t) \right) \mathrm{d}x \\
&= \int_a^b \left(u_x u_{xt} + v_x v_{xt} + (u_{xx}-v_t)u_t + (v_{xx}+u_t)v_t \right) \mathrm{d}x \\
&= \int_a^b (u_x u_t + v_x v_t)_x \, \mathrm{d}x \;=\; [u_x u_t + v_x v_t]_{x=a}^{x=b} \;=\; 0,
\end{aligned}
$$

because of the periodicity in space of u and v, and of their derivatives w.r.t. x. $\square$

We also consider the two quadratic functionals

$$
\mathcal{M}_1[u,v] = \int_a^b (u^2+v^2)\mathrm{d}x, \qquad \mathcal{M}_2[u,v] = \int_a^b (v_x u - u_x v)\mathrm{d}x, \qquad (6)
$$

representing the *mass* and the *momentum*. Also for such functionals, the following result holds true.

Theorem 2. *Under regularity assumptions on f and on the initial data, the two quadratic functionals (6) are constant along the solution of (3).*

<u>Proof</u>   In fact, from (3) and (6), one has:

$$
\begin{aligned}
\dot{\mathcal{M}}_1[u,v] &= 2\int_a^b (uu_t+vv_t)\,\mathrm{d}x \\
&= 2\int_a^b \left(-u(v_{xx}+f'(u^2+v^2)v) + v(u_{xx}+f'(u^2+v^2)u) \right) \mathrm{d}x \\
&= 2\int_a^b (vu_{xx} - uv_{xx} + u_x v_x - u_x v_x)\,\mathrm{d}x \\
&= 2\int_a^b (vu_x - uv_x)_x \mathrm{d}x \;=\; 2\left[vu_x - uv_x\right]_{x=a}^{x=b} \;=\; 0,
\end{aligned}
$$

---

[2] As is usual, the dot denotes the time derivative.

because of the periodicity in space. For the same reason, by considering that

$$0 = \int_a^b (u_t v)_x \mathrm{d}x = \int_a^b (u_{xt}v + u_t v_x)\mathrm{d}x \quad \Rightarrow \quad \int_a^b v u_{xt}\mathrm{d}x = -\int_a^b u_t v_x \mathrm{d}s,$$

$$0 = \int_a^b (v_t u)_x \mathrm{d}x = \int_a^b (v_{xt}u + v_t u_x)\mathrm{d}x \quad \Rightarrow \quad \int_a^b u v_{xt}\mathrm{d}x = -\int_a^b v_t u_x \mathrm{d}s,$$

one obtains, by virtue of (3):

$$
\begin{aligned}
\dot{\mathcal{M}}_2[u,v] &= \int_a^b (v_{xt}u + v_x u_t - u_{xt}v - u_x v_t)\,\mathrm{d}x = 2\int_a^b (v_x u_t - u_x v_t)\mathrm{d}x \\
&= 2\int_a^b \left(-v_x(v_{xx} + f'(u^2+v^2)v) - u_x(u_{xx} + f'(u^2+v^2)u)\right)\mathrm{d}x \\
&= -\int_a^b \left(u_x^2 + v_x^2 + f(u^2+v^2)\right)_x \mathrm{d}x = \left[u_x^2 + v_x^2 + f(u^2+v^2)\right]_{x=a}^{x=b} \\
&= 0.\ \square
\end{aligned}
$$

Remark 1. *It is worth stressing that the three invariants (5) and (6) have a special physical meaning:*

- *in the context of quantum mechanics they represent, respectively, total energy, mass, and momentum (from which their names);*

- *in the context of optics, they represent electromagnetic energy, power, and power current associated with the signal (see, e.g., [4]), respectively.*

Consequently, when numerically solving the problem it would be desirable their conservation (exact or approximate) to be inherited by the discrete solution.

In order for numerically solving problem (3), we shall at first consider a Fourier expansion in space of the solution. In particular, we consider the following orthonormal basis for $L^2[a,b]$, which takes into account of the periodicity in space:

$$
\begin{aligned}
c_0(x) &\equiv \frac{1}{\sqrt{b-a}}, \\
c_j(x) &= \sqrt{\frac{2}{b-a}}\cos\left(2j\pi\,\frac{x-a}{b-a}\right), \\
s_j(x) &= \sqrt{\frac{2}{b-a}}\sin\left(2j\pi\,\frac{x-a}{b-a}\right), \qquad j = 1, 2, \dots.
\end{aligned}
\tag{7}
$$

6

In so doing, one obtains, for suitable time dependent coefficients:

$$u(x,t) = \gamma_0(t)c_0(x) + \sum_{j\geq 1} \gamma_j(t)c_j(x) + \eta_j(t)s_j(x),$$

$$v(x,t) = \alpha_0(t)c_0(x) + \sum_{j\geq 1} \alpha_j(t)c_j(x) + \beta_j(t)s_j(x). \tag{8}$$

By introducing the infinite vectors

$$\boldsymbol{w}(x) = \begin{pmatrix} c_0(x) \\ c_1(x) \\ s_1(x) \\ c_2(x) \\ s_2(x) \\ \vdots \end{pmatrix}, \qquad \boldsymbol{q}(t) = \begin{pmatrix} \gamma_0(t) \\ \gamma_1(t) \\ \eta_1(t) \\ \gamma_2(t) \\ \eta_2(t) \\ \vdots \end{pmatrix}, \qquad \boldsymbol{p}(t) = \begin{pmatrix} \alpha_0(t) \\ \alpha_1(t) \\ \beta_1(t) \\ \alpha_2(t) \\ \beta_2(t) \\ \vdots \end{pmatrix}, \tag{9}$$

and the infinite matrix

$$D = \frac{2\pi}{b-a} \begin{pmatrix} 0 & & & & \\ & 1\cdot\begin{pmatrix} 1 & \\ & 1 \end{pmatrix} & & \\ & & 2\cdot\begin{pmatrix} 1 & \\ & 1 \end{pmatrix} & \\ & & & \ddots \end{pmatrix}, \tag{10}$$

we see that (8) can be rewritten as

$$u(x,t) = \boldsymbol{w}(x)^\top \boldsymbol{q}(t), \qquad v(x,t) = \boldsymbol{w}(x)^\top \boldsymbol{p}(t), \tag{11}$$

and the problem can be formulated as the infinite-dimensional Hamiltonian ODE problem:

$$\dot{\boldsymbol{q}} = D^2\boldsymbol{p} - \int_a^b \left[\boldsymbol{w}(x)f'\left((\boldsymbol{w}(x)^\top\boldsymbol{q})^2 + (\boldsymbol{w}(x)^\top\boldsymbol{p})^2\right)\boldsymbol{w}(x)^\top\boldsymbol{p} \right]\mathrm{d}x,$$

$$\dot{\boldsymbol{p}} = -D^2\boldsymbol{q} + \int_a^b \left[\boldsymbol{w}(x)f'\left((\boldsymbol{w}(x)^\top\boldsymbol{q})^2 + (\boldsymbol{w}(x)^\top\boldsymbol{p})^2\right)\boldsymbol{w}(x)^\top\boldsymbol{q} \right]\mathrm{d}x, \tag{12}$$

which is Hamiltonian with Hamiltonian function

$$H(\boldsymbol{q},\boldsymbol{p}) = \frac{1}{2}\left[\boldsymbol{p}^\top D^2\boldsymbol{p} + \boldsymbol{q}^\top D^2\boldsymbol{q} - \int_a^b f\left((\boldsymbol{w}(x)^\top\boldsymbol{q})^2 + (\boldsymbol{w}(x)^\top\boldsymbol{p})^2\right)\mathrm{d}x\right].$$

(13)

By also introducing the infinite matrix

$$\tilde{D} = \frac{2\pi}{b-a}\begin{pmatrix} 0 & & & & \\ & 1\cdot\begin{pmatrix} & -1 \\ 1 & \end{pmatrix} & & & \\ & & 2\cdot\begin{pmatrix} & -1 \\ 1 & \end{pmatrix} & \\ & & & \ddots \end{pmatrix},$$

(14)

such that

$$\tilde{D}\boldsymbol{w}(x) = \boldsymbol{w}'(x) \equiv \frac{2\pi}{b-a}\begin{pmatrix} 0, & -s_1(x), & c_1(x), & -2s_2(x), & 2c_2(x), & \dots \end{pmatrix}^\top,$$

the following result then holds true.

Theorem 3. *The Hamiltonian (13) is equivalent to the Hamiltonian functional (5). Similarly, the two quadratic functionals (6) are equivalent to*

$$M_1(\boldsymbol{q},\boldsymbol{p}) = \int_a^b\left[(\boldsymbol{w}(x)^\top\boldsymbol{q})^2 + (\boldsymbol{w}(x)^\top\boldsymbol{p})^2\right]\mathrm{d}x, \quad M_2(\boldsymbol{q},\boldsymbol{p}) = -2\boldsymbol{q}^\top\tilde{D}\boldsymbol{p}, \quad (15)$$

respectively. Consequently, they are conserved along the solution of (12).

<u>Proof</u> The equivalence of $\mathcal{H}$ and $\mathcal{M}_1$ with H and M_1, respectively, follows quite straightforwardly from (11). Concerning the last quadratic invariant, by considering that

$$u_x(x,t) = \left(\tilde{D}\boldsymbol{w}(x)\right)^\top\boldsymbol{q}(t), \qquad v_x(x,t) = \left(\tilde{D}\boldsymbol{w}(x)\right)^\top\boldsymbol{p}(t), \qquad \tilde{D}^\top = -\tilde{D},$$

and, because of the orthormality of the basis (7),

$$\int_a^b \boldsymbol{w}(x)\boldsymbol{w}(x)^\top\mathrm{d}x = I,$$

8

the identity operator, one obtains:

$$
\begin{aligned}
\mathcal{M}_2[u, v] &= \int_a^b [v_x u - u_x v] \mathrm{d}x \\
&= \int_a^b \left[(\tilde{D}\boldsymbol{w}(x))^\top \boldsymbol{p}\, \boldsymbol{q}^\top \boldsymbol{w}(x) - \boldsymbol{q}^\top (\tilde{D}\boldsymbol{w}(x))\, \boldsymbol{w}(x)^\top \boldsymbol{p} \right] \mathrm{d}x \\
&= -\int_a^b \left[\boldsymbol{q}^\top \boldsymbol{w}(x)\boldsymbol{w}(x)^\top \tilde{D}\boldsymbol{p} + \boldsymbol{q}^\top \tilde{D}\boldsymbol{w}(x)\boldsymbol{w}(x)^\top \boldsymbol{p} \right] \mathrm{d}x \\
&= -\boldsymbol{q}^\top \left[\int_a^b \boldsymbol{w}(x)\boldsymbol{w}(x)^\top \mathrm{d}x \right] \tilde{D}\boldsymbol{p} - \boldsymbol{q}^\top \tilde{D} \left[\int_a^b \boldsymbol{w}(x)\boldsymbol{w}(x)^\top \mathrm{d}x \right] \boldsymbol{p} \\
&= -2\boldsymbol{q}^\top \tilde{D}\boldsymbol{p} = M_2(\boldsymbol{q}, \boldsymbol{p}). \ \square
\end{aligned}
$$

As is clear, in order to obtain a practical computational procedure, the series in (8) have to be truncated to a finite sum, i.e., for a suitable large N:

$$
\begin{aligned}
u(x, t) &= \gamma_0(t)c_0(x) + \sum_{j=1}^N \gamma_j(t)c_j(x) + \eta_j(t)s_j(x), \\
v(x, t) &= \alpha_0(t)c_0(x) + \sum_{j=1}^N \alpha_j(t)c_j(x) + \beta_j(t)s_j(x),
\end{aligned}
\tag{16}
$$

where, for sake of brevity, we continue to use the same symbols to denote the truncated approximations. For each t, such functions will belong to the functional space

$$
\mathcal{V}_N = \operatorname{span}\left\{ c_0(x), c_1(x), s_1(x), \ldots, c_N(x), s_N(x) \right\}. \tag{17}
$$

Consequently, the dimension of the vectors and matrices (9)–(10) and (14) becomes $2N + 1$. As an example, matrix (10) now becomes:

$$
D = \frac{2\pi}{b-a} \begin{pmatrix} 0 & & & & \\ & 1 \cdot \begin{pmatrix} & 1 \\ 1 & \end{pmatrix} & & & \\ & & 2 \cdot \begin{pmatrix} & 1 \\ 1 & \end{pmatrix} & & \\ & & & \ddots & \\ & & & & N \cdot \begin{pmatrix} & 1 \\ 1 & \end{pmatrix} \end{pmatrix}, \tag{18}
$$

9

However, in this case, the approximations will no more satisfy, in general, the equations (12). Nevertheless, by requiring the residual be orthogonal to $\mathcal{V}_N$, one formally retrieves again the set of equations (12) which, however, has now dimension $4N + 2$. Such equations are still Hamiltonian with Hamiltonian function formally still given by (5). Moreover, also the truncated versions of (15) are still constants of motion. It can be proved (see, e.g., [28]) that, under regularity assumptions, the truncated version of the solution and of the invariants converge at least exponentially to the exact counterparts as $N \to \infty$ (spectral accuracy). In so doing, one obtains a Fourier-Galerkin space semi-discretization of the original problem (3).

We also observe that the integrals in (12) need to be computed. Nevertheless, since the argument is a periodic function, this can be done by using a composite trapezoidal rule, based at the discrete points

$$x_i = a + \frac{i}{m}(b - a), \qquad i = 0, 1, \ldots, m, \tag{19}$$

which allows, under regularity assumptions, to approximate the integrals within machine accuracy, by choosing m large enough (see [13] for details).[3]

As a result, the equations (12), with the truncated expansions (16), along with the approximation of the involved integrals on the abscissae (19), define the semi-discrete Hamiltonian problem to be solved in time. In the next sections we shall consider its numerical solution.

3. Hamiltonan Boundary Value Methods

In this section, we sketch the basic facts concerning Hamiltonian Boundary Value Methods (HBVMs), which are a class of energy-conserving Runge-Kutta methods, recently devised for the efficient numerical solution of Hamiltonian systems [24, 17, 18, 21, 22] (see also the monograph [16]).

Let then

$$\dot{y} = J\nabla H(y), \qquad y(0) = y_0, \qquad J^\top = -J, \tag{20}$$

be a Hamiltonian problem we want to solve, which is defined by the (autonomous) Hamiltonian H. Having fixed a stepsize $h > 0$, we look for a numerical method defining a suitable path σ such that:

$$\sigma(0) = y_0, \qquad \sigma(h) =: y_1, \qquad H(y_1) = H(y_0). \tag{21}$$

---

[3]In general, m is conveniently chosen in the form $m = \ell N + 1$, for a suitable $\ell \in \mathbb{N}$.

Namely, the new approximation $y_1 \approx y(h)$ satisfies the energy conservation property. In particular, we look for $\sigma \in \Pi_s$ [4] and, by considering the scaled orthonormal Legendre basis $\{P_j\}_{j\geq 0}$ for $L^2[0,1]$,

$$P_j \in \Pi_j, \qquad \int_0^1 P_i(x)P_j(x)\mathrm{d}x = \delta_{ij}, \qquad \forall i,j = 0,1,\ldots, \qquad (22)$$

with δ_{ij} the Kronecker delta, we define the expansion

$$\dot\sigma(ch) = \sum_{j=0}^{s-1} P_j(c)\gamma_j, \qquad c \in [0,1], \qquad (23)$$

for suitable coefficients $\{\gamma_j\}$ to be determined. By imposing the first condition in (21), we obtain

$$\sigma(ch) = y_0 + h\sum_{j=0}^{s-1} \int_0^c P_j(x)\mathrm{d}x\, \gamma_j, \qquad c \in [0,1]. \qquad (24)$$

Consequently, from (22) and considering that $P_0(x) \equiv 1$, one has (see the second expression in (21)):

$$y_1 \equiv \sigma(h) = y_0 + h\gamma_0. \qquad (25)$$

The coefficients $\gamma_0,\ldots,\gamma_{s-1}$ are then determined by imposing the last requirement in (21), i.e., energy-conservation: this will be done by resorting to a *line integral approach*. In more details, from (20)–(24), one has:

$$
\begin{aligned}
0 &= H(y_1) - H(y_0) = H(\sigma(h)) - H(\sigma(0)) = \int_0^h \nabla H(\sigma(t))^\top \dot\sigma(t)\mathrm{d}t \\
&= h\int_0^1 \nabla H(\sigma(ch))^\top \dot\sigma(ch)\mathrm{d}c = h\int_0^1 \nabla H(\sigma(ch))^\top \sum_{j=0}^{s-1} P_j(c)\gamma_j\,\mathrm{d}c \\
&= h\sum_{j=0}^{s-1} \left[\int_0^1 \nabla H(\sigma(ch))P_j(c)\mathrm{d}c\right]^\top \gamma_j,
\end{aligned}
$$

which holds clearly true, by virtue of the skew-symmetry of J, by setting

$$\gamma_j = \int_0^1 J\nabla H(\sigma(ch))P_j(c)\mathrm{d}c, \qquad j = 0,\ldots,s-1. \qquad (26)$$

---

[4]As is usual, Π_s denotes the vector space of polynomials of degree s.

11

Approximating such integrals by means of a suitable quadrature formula, provides us with HBVMs. In more details, by considering the Gauss formula based at the k Legendre nodes, i.e.

$$P_k(c_i) = 0, \qquad i = 1, \ldots, k,$$

so that equation (26) is replaced by

$$\gamma_j = \sum_{\ell=1}^{k} b_\ell J \nabla H(Y_\ell) P_j(c_\ell), \qquad j = 0, \ldots, s-1, \tag{27}$$

with $b_1, \ldots, b_k$ the Legendre weights, one derives the method HBVM(k, s).[5] The resulting method may be shown to be actually a k-stage Runge-Kutta method, with stages

$$Y_i := \sigma(c_i h) = y_0 + h \sum_{j=0}^{s-1} \int_0^{c_i} P_j(x) \mathrm{d}x \sum_{\ell=1}^{k} b_\ell J \nabla H(Y_\ell) P_j(c_\ell), \qquad i = 1, \ldots, k, \tag{28}$$

and the new approximation given by:

$$y_1 = y_0 + h \sum_{i=1}^{k} b_i J \nabla H(Y_i). \tag{29}$$

From (28)-(29) one derives that HBVM(k, s) is the k-stage Runge-Kutta method with Butcher tableau

$$\frac{\boldsymbol{c} \mid \mathcal{I}_s \mathcal{P}_s^\top \Omega}{\boldsymbol{b}^\top}, \tag{30}$$

with $\boldsymbol{b} = \left(\begin{array}{ccc} b_1, & \ldots, & b_k \end{array} \right)^\top$, $\boldsymbol{c} = \left(\begin{array}{ccc} c_1, & \ldots, & c_k \end{array} \right)^\top$,

$$\mathcal{I}_s = \left(\int_0^{c_i} P_{j-1}(x) \mathrm{d}x \right)_{ij}, \quad \mathcal{P}_s = \left(P_{j-1}(c_i) \right)_{ij} \in \mathbb{R}^{k \times s}, \tag{31}$$

and

$$\Omega = \begin{pmatrix} b_1 & & \\ & \ddots & \\ & & b_k \end{pmatrix}. \tag{32}$$

The following result holds true.

---

[5]Different quadratures can be also considered, as is shown, e.g., in [24].

Theorem 4. *Under suitable regularity assumptions on H, for all $k \geq s$ a HBVM(k, s) method:*

- *is symmetric and has order $2s$;*

- *for $k = s$ it reduces to the (symplectic) s-stage Gauss-collocation method;*

- *is energy-conserving for all polynomial Hamiltonians H of degree no larger than $2k/s$;*

- *for general Hamiltonians, $H(y_1) = H(y_0) + O(h^{2k+1})$.*

<u>Proof</u>   See, e.g., [22]. $\square$

We observe that, from the last point of Theorem 4, even in the non-polynomial case one can always gain a *practical* energy conservation, by choosing k large enough. This, in turn, is not a big issue since, as we are going to see in the next section, the discrete problem to be solved at each step has *always* (block) dimension s, *independently* of k.

4. Implementation of the methods

We here explain the efficient implementation of HBVM(k, s): even though this issue has been the subject of previous investigations [10, 11, 16, 20], nevertheless, we report here the main facts, also considering that the general approach will be suitably adapted to the efficient solution of problem (12).

The natural implementation of the HBVM(k, s) method, cast as the k-stage Runge-Kutta method with tableau (30), would result in the solution, at each integration step, of the nonlinear system of equations in the k stages:

$$Y := \begin{pmatrix} Y_1 \\ \vdots \\ Y_k \end{pmatrix} = e \otimes y_0 + h \left(\mathcal{I}_s \mathcal{P}_s^\top \Omega \otimes J \right) \nabla H(Y),$$

with $e = \begin{pmatrix} 1, & \ldots, & 1 \end{pmatrix}^\top \in \mathbb{R}^k$, and an obvious meaning of $\nabla H(Y)$. Nevertheless, whichever k, one can always recast the discrete problem in term of the s coefficients (27) of the polynomial σ. This results in [20]

$$\gamma := \begin{pmatrix} \gamma_0 \\ \vdots \\ \gamma_{s-1} \end{pmatrix} = \left(\mathcal{P}_s^\top \Omega \otimes J \right) \nabla H(Y).$$

Summing up the last two equations, one eventually obtains the discrete problem [6]

$$G(\boldsymbol{\gamma}) := \boldsymbol{\gamma} - \left(\mathcal{P}_s^\top \Omega \otimes J\right) \nabla H \left(\boldsymbol{e} \otimes y_0 + h\mathcal{I}_s \otimes I \boldsymbol{\gamma}\right) = \mathbf{0}, \qquad (33)$$

whose (block) dimension is s, independently of k. In order for efficiently solving (33), one can use the simplified Newton method which, by taking into account that [20]

$$\mathcal{P}_s^\top \Omega \mathcal{I}_s = X_s := \begin{pmatrix} \frac{1}{2} & -\xi_1 & & \\ \xi_1 & 0 & \ddots & \\ & \ddots & \ddots & -\xi_{s-1} \\ & & \xi_{s-1} & 0 \end{pmatrix} \in \mathbb{R}^{s \times s}, \qquad \xi_i = \frac{1}{2\sqrt{4i^2 - 1}},$$

$$(34)$$

results in the iteration

$$\begin{aligned} \text{for } \ell = 0, 1, \dots \quad &: \\ \text{solve} \quad &: \quad (I - hX_s \otimes J\nabla^2 H_0)\boldsymbol{\delta}^\ell = -G(\boldsymbol{\gamma}^\ell) \\ \text{update} \quad &: \quad \boldsymbol{\gamma}^{\ell+1} = \boldsymbol{\gamma}^\ell + \boldsymbol{\delta}^\ell \end{aligned}$$

where $\nabla^2 H_0 = \nabla^2 H(y_0)$.[7] Even though the coefficient matrix is the same during the whole iteration, its size is s times that of the continuous problem to be solved, thus resulting in a possibly costly iteration. In order to get rid of this problem, in [20] a *blended iteration* has been considered. This approach, which has been at first proposed in [9, 25], has already been successfully implemented in the computational codes `BiM` [26] and `BIMD` [27]. The resulting iteration is as follows (we refer to [16, 20] for full details):

$$\begin{aligned} \text{set} \quad &: \quad \rho_s = \min\{|\lambda| : \lambda \text{ eigenvalue of } X_s\} \\ \text{set} \quad &: \quad M = I - h\rho_s J\nabla^2 H_0 \qquad\qquad (35) \\ \text{for } \ell = 0, 1, \dots \quad &: \\ \text{set} \quad &: \quad \boldsymbol{\eta}^\ell = -G(\boldsymbol{\gamma}^\ell), \quad \boldsymbol{\eta}_1^\ell = (\rho_s X_s^{-1} \otimes I)\boldsymbol{\eta}^\ell \\ \text{solve} \quad &: \quad (I_s \otimes M)\boldsymbol{u}^\ell = \boldsymbol{\eta}^\ell - \boldsymbol{\eta}_1^\ell \\ \text{solve} \quad &: \quad (I_s \otimes M)\boldsymbol{\delta}^\ell = \boldsymbol{\eta}_1^\ell + \boldsymbol{u}^\ell \\ \text{update} \quad &: \quad \boldsymbol{\gamma}^{\ell+1} = \boldsymbol{\gamma}^\ell + \boldsymbol{\delta}^\ell \end{aligned}$$

---

[6]When not explicitly specified, hereafter the dimension of the identity matrix I is unambiguously deduced from the context.

[7]Moreover, one usually takes the initial guess $\boldsymbol{\gamma}^0 = \mathbf{0}$.

As is clear, now only the factorization of matrix M defined at (35) is needed, thus greatly reducing the cost per iteration.

A further substantial improvement can be gained when considering the solution of problem (12), whose dimension is $4N + 2$. In fact, by assuming that the solution is bounded and (see (18))

$$\|f'\|, \|f''\| \ll \|D^2\| = \left(\frac{2\pi N}{b - a}\right)^2,$$

one easily obtains that, in such a case, matrix M can be approximated as

$$M \approx M_0 := \left(\begin{array}{cc} I_{2N+1} & -h\rho_s D^2 \\ h\rho_s D^2 & I_{2N+1} \end{array}\right). \tag{36}$$

Matrix M_0 has the following important features:

- it is independent of the current step;

- it is a 2×2 block matrix, with *diagonal* blocks of dimension $2N + 1$.

Moreover, the following result holds true.

Theorem 5. *Matrix M_0 is nonsingular, and*

$$M_0^{-1} = \left(\begin{array}{cc} (I_{2N+1} + B^2)^{-1} & B(I_{2N+1} + B^2)^{-1} \\ -B(I_{2N+1} + B^2)^{-1} & (I_{2N+1} + B^2)^{-1} \end{array}\right), \qquad B = h\rho_s D^2. \tag{37}$$

<u>Proof</u> In fact, one obtains:

$$\left(\begin{array}{cc} I_{2N+1} & -B \\ B & I_{2N+1} \end{array}\right) \cdot \left(\begin{array}{cc} (I_{2N+1} + B^2)^{-1} & B(I_{2N+1} + B^2)^{-1} \\ -B(I_{2N+1} + B^2)^{-1} & (I_{2N+1} + B^2)^{-1} \end{array}\right)$$

$$= \left(\begin{array}{cc} I_{2N+1} & \\ & I_{2N+1} \end{array}\right). \;\square$$

The result of Theorem 5 allows us to recast the blended iteration (35) for solving (12) in a simplified (and more efficient) form, as follows:

$$
\begin{aligned}
\text{set} \quad &: \quad \rho_s = \min\{|\lambda| : \lambda \text{ eigenvalue of } X_s\} \\
\text{set} \quad &: \quad M_0^{-1} \quad \text{as in (37)} \\
\text{for } \ell = 0, 1, \ldots \quad &: \\
\text{set} \quad &: \quad \boldsymbol{\eta}^\ell = -G(\boldsymbol{\gamma}^\ell), \quad \boldsymbol{\eta}_1^\ell = (\rho_s X_s^{-1} \otimes I_{2N+1}) \boldsymbol{\eta}^\ell \\
\text{set} \quad &: \quad \boldsymbol{u}^\ell = (I_s \otimes M_0^{-1}) (\boldsymbol{\eta}^\ell - \boldsymbol{\eta}_1^\ell) \\
\text{set} \quad &: \quad \boldsymbol{\delta}^\ell = (I_s \otimes M_0^{-1}) (\boldsymbol{\eta}_1^\ell + \boldsymbol{u}^\ell) \\
\text{update} \quad &: \quad \boldsymbol{\gamma}^{\ell+1} = \boldsymbol{\gamma}^\ell + \boldsymbol{\delta}^\ell
\end{aligned} \tag{38}
$$

From this algorithm, one clearly deduces the following facts:

- matrix M_0^{-1} is built only once and, moreover, it can be stored into two diagonal matrices (i.e., vectors), of dimension $2N + 1$. That is, $(I_{2N+1} + B^2)^{-1}$ and $B(I_{2N+1} + B^2)^{-1}$;

- the complexity of the linear algebra in the improved iteration is *linear* in $s(2N + 1)$;

- on the other hand, the complexity of the evaluation of G (see (33)) is proportional to the product $sk(2N + 1)$. Moreover, it requires k function evaluations of the right-hand side of (12). In turn, a function evaluation has a cost which is proportional to m, where $m + 1$ (see (19)) is the number of grid points used for approximating the involved integrals.

Overall, one concludes that the cost per iteration is *linear* in the number of terms of the truncated expansion (16).

5. Numerical tests

In this section, we aim to give evidence of the various theoretical aspects mentioned above.

Spectral accuracy

Let us consider the problem (1) with

$$b = -a = 10, \qquad f(\zeta) = -\frac{1}{2}\zeta^6, \qquad \psi(x,0) = e^{-x^2} + i\,e^{-(x-1)^2}. \qquad (39)$$

We now consider the accuracy of the truncated Hamiltonian H, of the quadratic invariants M_1 and M_2, and of the initial data, depending on the number N of terms in the truncated expansions (16). In particular, we computed the initial truncated Hamiltonian for $N = 10, 20, 30, 40, 50$ (the involved integrals are computed by using the composite trapezoidal rule with $m = 250$ (see (19))), along with the truncated quadratic integrals. We also computed the maximum error in the initial data, E_0, once it is projected into the subspace (17). The actual values of the invariants are:

$$H \approx 2.1931, \qquad M_1 \approx 2.5066, \qquad M_2 \approx -0.0760.$$
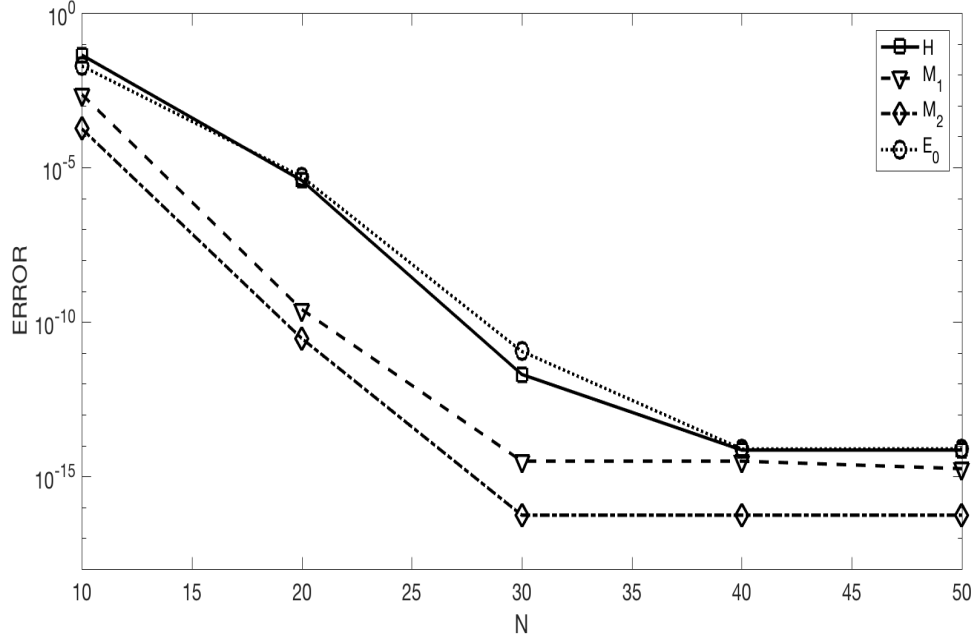
Figure 1: Accuracy of the truncated Fourier expansion (16): errors in the truncated Hamiltonian (solid line and squares); truncated mass (dashed line and triangles); truncated momentum (dash-dotted line and diamonds); errors on the initial data (dotted line and circles).

Figure 1 summarizes the obtained results for H, M_1, M_2, and E_0. In particular, one has that the error decreases exponentially in N (at least), thus confirming the phenomenon of spectral accuracy.

Approximation of the invariants

We now consider the same problem (1)-(39) with $T = 10$. We solve it by using the methods HBVM(k,s), with $k \geq s$, aiming at showing that:

- all methods have order $2s$;

- for $k = s$ one has the s-stage symplectic Gauss collocation method, so that one expects the quadratic invariants M_1 and M_2 to be exactly conserved, with the Hamiltonian conserved up to order $2s$;

17

- for $k > s$ one has that the Hamiltonian is conserved up to order $2k$ (until round-off is reached), whereas the two quadratic invariants are conserved up to order $2s$.

In the numerical tests, we shall consider decreasing time-steps h, having fixed (see (16) and (19)) $N = 50$ and $m = 250$. The maximum error on the solution is numerically estimated via the doubling of the time mesh. The previous statements are duly confirmed by the figures in Tables 1–4, for the case $s = 1$, and Tables 5–6, for the case $s = 2$.

In addition to this, it is worth noticing that no appreciable drift can be observed in the numerical invariants. This is confirmed by the plots in Figure 2, with the errors in the three invariants H, M_1, and M_2, for the implicit mid-point (i.e., HBVM(1,1)) and the HBVM(8,1) methods when solving the above problem with time-step $h = 0.1$ on the interval $[0, 10^3]$: the former a symplectic method, the latter a (practically) energy-conserving one, for the given time-step h.

Computational cost

In this subsection, we compare the previous methods in terms of mean number of iterations for getting convergence (we remind that the nonlinear iteration (38) is performed until round-off). In more details, in Table 7 we list the mean number of iterations per step to reach full convergence, for the considered couples of (k, s) and decreasing values of the time-step h. As one may see, the iterations decrease with the time-step and essentially depends only on s.

Conservation of the Hamiltonian

In some situations, the conservation of the energy may result in a more robust numerical method. In particular, in the previous example (39), the function $f(\zeta)$ was *non positive*. This, in turn, in view of the Hamiltonian function (4), implies the boundedness of the solution. Consequently, provided that the discrete Hamiltonian (13) is conserved (even approximately), also the discrete solution will be bounded. Conversely, when $f(\zeta)$ is a *non negative* function, a blow-up in finite time may occur, depending on the initial condition and, in such a case, a more precise conservation of H could be

useful. This is, in fact, the case for the problem defined by

$$b = -a = 20, \qquad f(\zeta) = 0.2526896 \cdot \zeta^6, \qquad \psi(x, 0) = \frac{1}{\cosh(x)}. \qquad (40)$$

With such parameters, one obtains

$$H \approx 0.24, \qquad M_1 = 2, \qquad M_2 = 0,$$

and moreover, the solution has a blow-up at about $t = 2$, as is shown in Figure 3,[8] containing the plot of $|\psi(x, t)|^2$. We solve the problem by means of the symplectic 2-stage Gauss method (i.e., HBVM(2,2)) and the (practically) energy-conserving HBVM(8,2) method (both methods are fourth-order), with parameters:

$$N = 100, \qquad m = 400, \qquad h = 0.1, \qquad nsteps = 1000. \qquad (41)$$

In so doing, one obtains that the error in the initial data is $E_0 \approx 10^{-10}$. Moreover:

- for the 2-stage Gauss method, one obtains the solution depicted in the upper plot in Figure 4, with all the 1000 steps performed, the two quadratic invariants are exactly preserved, and the Hamiltonian error is $\approx 2 \cdot 10^{-6}$;

- for the HBVM(8,2) method, one obtains the solution depicted in the lower plot in Figure 4. In such a case, the nonlinear iteration breaks down after 20 steps, with H and M_2 exactly conserved, and an error in M_1 which is $\approx 2 \cdot 10^{-4}$.

As one may clearly see, the solution provided by the 2-stage Gauss method is wrong, even though the two quadratic invariants are exactly conserved, whereas the solution of the energy-conserving HBVM(8,2) method is qualitatively correct.

---

[8]This reference solution has been computed by using a higher order method with a much smaller time-step, over a finer space semi-discretization.

6. Concluding remarks

In this paper, we studied the numerical solution of the nonlinear Schrödinger equation, showing that the Hamiltonian ODE problem deriving from its Fourier-Galerkin space semi-discretization can be conveniently solved by means of energy-conserving methods in the class of HBVMs. In particular, in some circumstances, the use of energy-conserving methods may confer more robustness on the numerical solution.

We plan to extend this approach to different space semi-discretizations, as well as to different kinds of *line integral methods.* In particular, the EQUIP methods studied in [19, 23, 15, 16], being energy conserving and defined by a symplectic Runge-Kutta map at each step, would be able to conserve both the energy and the quadratic invariants of the semi-discrete Hamiltonian problem.

References

[1] M.J. Ablowitz, H. Segur. *Solitons and the Inverse Scattering Transform.* SIAM, Philadelphia, 1981.

[2] G.B. Agrawal. *Nonlinear fiber optics* (third edition). Academic Press, London, 2001.

[3] D. Bambusi, E. Faou, B. Grébert. Existence and stability of solitons for fully discrete approximations of the nonlinear Schrodinger equation. *Numer. Math.* **123** (2013) 461–492.

[4] L. Barletti, M. Secondini. Signal-noise interaction in nonlinear optical fibers: a hydrodynamic approach. *Optics Express* **23** (2015) 27419–27433.

[5] L. Barletti, L. Brugnano, G. Frasca Caccia, F. Iavernaro. Recent advances in the numerical solution of Hamiltonian partial differential equations. *AIP Conf. Proc.* **1776** (2016) 020002.

[6] G. Benettin, A. Giorgilli. On the Hamiltonian interpolation of near to the identity symplectic mappings with application to symplectic integration algorithms. *J. Statist. Phys.* **74** (1994) 1117–1143.

[7] T.J. Bridges, S. Reich. Multi-symplectic integrators: Numerical schemes for Hamiltonian PDEs that conserve symplecticity. *Physics Letters A* **284** (2001) 184–193.

[8] T.J. Bridges, S. Reich. Numerical methods for Hamiltonian PDEs. *J. Phys. A: Math. Gen.* **39** (2006) 5287–5320.

[9] L. Brugnano. Blended Block BVMs (B3VMs): A Family of Economical Implicit Methods for ODEs. *Jour. Comput. Appl. Math.* **116** (2000) 41–62.

[10] L. Brugnano, G. Frasca Caccia, F. Iavernaro. Efficient implementation of geometric integrators for separable Hamiltonian problems. *AIP Conference Proc.* **1588** (2013) 734–737.

[11] L. Brugnano, G. Frasca Caccia, F. Iavernaro. Efficient implementation of Gauss collocation and Hamiltonian Boundary Value Methods. *Numer. Algorithms* **65** (2014) 633–650.

[12] L. Brugnano, G. Frasca Caccia, F. Iavernaro. Energy conservation issues in the numerical solution of Hamiltonian PDEs. *AIP Conference Proc.* **1648** (2015) p. 020002.

[13] L. Brugnano, G. Frasca Caccia, F. Iavernaro. Recent advances in the numerical solution of Hamiltonian PDEs. *AIP Conf. Proceed.* **1648** (2015) p. 150008.

[14] L. Brugnano, G. Frasca Caccia, F. Iavernaro. Energy conservation issues in the numerical solution of the semilinear wave equation. *Appl. Math. Comput.* **270** (2015) 842–870.

[15] L. Brugnano, G. Frasca Caccia, F. Iavernaro. Energy and QUadratic Invariants Preserving (EQUIP) methods for Hamiltonian Systems. *AIP Conference Proc.* **1738** (2016) 100002.

[16] L. Brugnano, F. Iavernaro. *Line Integral Methods for Conservative Problems.* CRC Press, Boca Raton, FL, 2016.

[17] L. Brugnano, F. Iavernaro, D. Trigiante. Hamiltonian BVMs (HBVMs): a family of "drift-free" methods for integrating polynomial Hamiltonian systems. *AIP Conf. Proc.* **1168** (2009) 715–718.

[18] L. Brugnano, F. Iavernaro, D. Trigiante. Hamiltonian Boundary Value Methods (energy preserving discrete line methods). *J. Numer. Anal. Ind. Appl. Math.* **5**(1–2) (2010) 17–37.

[19] L. Brugnano, F. Iavernaro, D. Trigiante. Energy and quadratic invariants preserving integrators of Gaussian type. *AIP Conf. Proc.* **1281** (2010) 227–230.

[20] L. Brugnano, F. Iavernaro, D. Trigiante. A note on the efficient implementation of Hamiltonian BVMs. *J. Comput. Appl. Math.* **236** (2011) 375–383.

[21] L. Brugnano, F. Iavernaro, D. Trigiante. The lack of continuity and the

role of infinite and infinitesimal in numerical methods for ODEs: the case of symplecticity. *Appl. Math. Comput.* **218** (2012) 8053–8063.

[22] L. Brugnano, F. Iavernaro, D. Trigiante. A simple framework for the derivation and analysis of effective one-step methods for ODEs. *Appl. Math. Comput.* **218** (2012) 8475–8485.

[23] L. Brugnano, F. Iavernaro, D. Trigiante. Energy and quadratic invariants preserving integrators based upon Gauss collocation formulae. *SIAM J. Numer. Anal.* **50**(6) (2012) 2897–2916.

[24] L. Brugnano, F. Iavernaro, D. Trigiante. Analysis of Hamiltonian Boundary Value Methods (HBVMs): a class of energy-preserving Runge–Kutta methods for the numerical solution of polynomial Hamiltonian systems. *Commun. Nonlin. Sci. Numer. Simul.* **20** (2015) 650–667.

[25] L. Brugnano, C. Magherini. Blended implementation of block implicit methods for ODEs. *Appl. Numer. Math.* **42** (2002) 29–45.

[26] L. Brugnano, C. Magherini. The BIM code for the numerical solution of ODES. *J. Comput. Appl. Math.* **164-165** (2004) 145–158.

[27] L. Brugnano, C. Magherini, F. Mugnai. Blended Implicit Methods for the Numerical Solution of DAE Problems. *J. Comput. Appl. Math.* **189** (2006) 34–50.

[28] C. Canuto, M.Y. Hussaini, A. Quarteroni, T.A. Zang. *Spectral Methods in Fluid Dynamics.* Springer-Verlag, New York, 1988.

[29] T. Cazenave. *Semilinear Schrödinger Equations.* American Mathematical Society, Providence R.I., 2003.

[30] J.B. Chen, M.Z. Qin. Multi-symplectic Fourier pseudospectral method for the nonlinear Schrödinger equation. *Electron. Trans. Numer. Anal.* **12** (2001) 193–204.

[31] J.B. Chen, M.Z. Qin. A multisymplectic variational integrator for the nonlinear Schrödinger equation. *Numer. Meth. Part. Differ. Equ.* **18** (2002) 523–536.

[32] J.B. Chen, M.Z. Qin, Y.F. Tang. Symplectic and multi-symplectic methods for the nonlinear Schrödinger equation. *Comput. Math. Appl.* **43** (2002) 1095–1106.

[33] R.Y. Chiao, E. Garmire, C.H. Townes. Self-trapping of optical beams. *Phys. Rev. Lett.* **13** (1965) 479.

[34] F. Dalfovo, S. Giorgini, L.P. Pitaevskii, S. Stringari. Theory of Bose-Einstein condensation in trapped gases. *Rev. Mod. Phys.* **71** (1999) 463–

512.

[35] A. Degasperis. Onde Nonlineari e Solitoni. Lecture notes, Università La Sapienza, Rome, 2008.

[36] M. Delfour, M. Fortin, G. Payr. Finite-difference solutions of a non-linear Schrödinger equation. *J. Comp. Phys.* **44**(2) (1981) 277–288.

[37] E. Faou. *Geometric Numerical Integration and Schrödinger Equations.* European Mathematical Society, 2012.

[38] E. Faou, B. Grébert, E. Paturel. Birkhoff normal form for splitting methods applied to semilinear Hamiltonian PDEs. Part I. Finite-dimensional discretization. *Numer. Math.* **114** (2010) 459–490.

[39] L. Gauckler, C. Lubich. Splitting Integrators for Nonlinear Schrödinger Equations Over Long Times *Found. Comput. Math.* **10** (2010) 275–302.

[40] H. Guan, Y. Jiao, J. Liu, Y. Tang. Explicit symplectic methods for the nonlinear Schrödinger equation. *Commun. Comput. Phys.* **6** (2009) 639-654.

[41] L. Guo, Y. Xu. Energy Conserving Local Discontinuous Galerkin Methods for the Nonlinear Schrödinger Equation with Wave Operator. *Journal of Scientific Computing* **65**(2) (2015) 622–647.

[42] E. Hairer, C. Lubich, G. Wanner. *Geometric Numerical Integration. Structure-Preserving Algorithms for Ordinary Differential Equations*, Second ed., Springer, Berlin, 2006.

[43] A. Hasegawa, T. Nyu. Eigenvalue communication. *IEEE J. Lightw. Technol.* **11** (1993) 395–399.

[44] C. Heitzinger, C. Ringhofer. A note on the symplectic integration of the nonlinear Schrdinger equation. *J. Comput. Electr.* **3**(1) (2004) 33–44.

[45] J. Hong, Y. Liu. A novel numerical approach to simulating nonlinear Schrödinger equations with varying coefficients. *Appl. Math. Lett.* **16** (2003) 759–765.

[46] A.L. Islas, D.A. Karpeev, C.M. Schober. Geometric integrators for the nonlinear Schrödinger equation. *J. Comput. Phys.* **173** (2001) 116–148.

[47] A.L. Islas, C.M. Schober. On the preservation of phase space structure under multisymplectic discretization. *J. Comput. Phys.* **197** (2004) 585–609.

[48] A.L. Islas, C.M. Schober. Backward error analysis for multisymplectic discretizations of Hamiltonian PDEs. *Math. Comp. Simul.* **69** (2005) 290–303.

[49] B. Leimkulher, S. Reich, *Simulating Hamiltonian Dynamics*. Cambridge University Press, 2004.

[50] C. Lubich. On splitting methods for Schrödinger-Poisson and cubic nonlinear Schrödinger equations. *Math. Comp.* **77** (2008) 2141–2153.

[51] I. Mitra, S. Roy. Relevance of quantum mechanics in circuit implementation of ion channels in brain dynamics. *Preprint*, arXiv: q-bio/0606008.

[52] A. Osborne. *Nonlinear Ocean Waves and the Inverse Scattering Transform.* Academic Press, Burlington, MA, 2010.

[53] H.L. Pécseli. *Waves and Oscillations in Plasmas.* CRC Press, Boca Raton, FL, 2013.

[54] L.P. Pitaevskii, S. Stringari. *Bose-Einstein Condensation.* Oxford University Press, New York, 2003.

[55] J.M. Sanz-Serna. Methods for the numerical solution of the nonlinear Schrödinger equation. *Math. Comp.* **43**(167) (1984) 21–27.

[56] J.M. Sanz-Serna, M.P. Calvo. *Numerical Hamiltonian problems*. Chapman & Hall, London, 1994.

[57] J.M. Sanz-Serna, V.S. Manoranjan. A method for the integration in time of certain partial differential equations. *J. Comp. Phys.* **52**(2) (1983) 273–289.

[58] Y.F. Tang, L. Vázquez, F. Zhang, V.M. Pérez-García. Symplectic methods for the nonlinear Schrdinger equation. *Comp. & Math. with Appl.* **32**(5)(1996) 73–83.

[59] Y. Tourigny, J.M. Sanz-Serna. The Numerical Study of Blowup with Application to a Nonlinear Schrödinger Equation. *Journal of Computational Physics* **102** (1992) 407–416.

[60] J.A.C. Weideman, B.M. Herbst. Split-step methods for the solution of the nonlinear Schrödinger equation. *SIAM J. Numer. Anal.* **23** (1986), 485–507.

[61] M.I. Yousefi, F.R. Kschischang. Information Transmission Using the Nonlinear Fourier Transform, Part I: Mathematical Tools. *IEEE Transactions on Information Theory* **60** (2014) 4312–4328.

[62] V.E. Zakharov, A.B. Shabat. Exact theory of two-dimensional selffocusing and one-dimensional self-modulation of wave in nonlinear media. *Soviet J. Exp. Theory Phys.* **34** (1972) 62–69.

Table 1: $k = s = 1$.

h	H-error	rate	M_1-error	M_2-error	solution error	rate
1.0000e-01	1.5263e-01	–	3.5527e-15	1.1102e-16	3.1647e-01	–
5.0000e-02	5.4933e-02	1.47	3.1086e-15	8.3267e-17	2.1236e-01	0.58
2.5000e-02	1.6073e-02	1.77	5.3291e-15	9.7145e-17	1.1841e-01	0.84
1.2500e-02	4.2411e-03	1.92	5.7732e-15	1.8041e-16	7.2974e-02	0.70
6.2500e-03	1.0834e-03	1.97	4.8850e-15	6.9389e-17	3.8272e-02	0.93
3.1250e-03	2.7399e-04	1.98	4.4409e-15	8.3267e-17	1.4807e-02	1.37
1.5625e-03	6.8749e-05	1.99	1.0658e-14	1.9429e-16	4.7065e-03	1.65
7.8125e-04	1.7199e-05	2.00	1.1102e-14	1.5266e-16	1.2715e-03	1.89

Table 2: $k = 2, s = 1$.

h	H-error	rate	M_1-error	rate	M_2-error	rate	solution error	rate
1.0000e-01	7.7440e-03	–	4.4228e-02	–	6.8433e-04	–	3.3727e-01	–
5.0000e-02	9.9802e-04	2.96	1.4068e-02	1.65	1.7293e-04	1.98	2.1560e-01	0.65
2.5000e-02	8.4482e-05	3.56	3.8528e-03	1.87	4.2546e-05	2.02	1.1837e-01	0.86
1.2500e-02	5.8796e-06	3.84	9.9038e-04	1.96	1.0776e-05	1.98	7.3826e-02	0.68
6.2500e-03	3.7958e-07	3.95	2.4973e-04	1.99	2.8205e-06	1.93	3.7448e-02	0.98
3.1250e-03	2.4044e-08	3.98	6.2607e-05	2.00	7.3188e-07	1.95	1.4685e-02	1.35
1.5625e-03	1.5091e-09	3.99	1.5663e-05	2.00	1.8490e-07	1.98	4.6908e-03	1.65
7.8125e-04	9.4400e-11	4.00	3.9163e-06	2.00	4.6296e-08	2.00	1.2625e-03	1.89

Table 3: $k = 3, s = 1$.

h	H-error	rate	M_1-error	rate	M_2-error	rate	solution error	rate
1.0000e-01	1.6584e-04	–	4.6712e-02	–	7.2022e-04	–	3.3837e-01	–
5.0000e-02	8.5550e-06	4.28	1.4336e-02	1.70	1.7617e-04	2.03	2.1567e-01	0.65
2.5000e-02	2.2872e-07	5.23	3.8738e-03	1.89	4.2801e-05	2.04	1.1837e-01	0.87
1.2500e-02	4.3306e-09	5.72	9.9179e-04	1.97	1.0794e-05	1.99	7.3826e-02	0.68
6.2500e-03	7.1244e-11	5.96	2.4982e-04	1.99	2.8216e-06	1.94	3.7448e-02	0.98
3.1250e-03	1.1289e-12	5.98	6.2612e-05	2.00	7.3195e-07	1.95	1.4685e-02	1.35
1.5625e-03	1.7319e-14	6.03	1.5663e-05	2.00	1.8490e-07	1.99	4.6908e-03	1.65
7.8125e-04	7.1054e-15	**	3.9163e-06	2.00	4.6297e-08	2.00	1.2625e-03	1.89

Table 4: $k = 4, s = 1$.

h	H-error	rate	M_1-error	rate	M_2-error	rate	solution error	rate
1.0000e-01	1.6354e-06	–	4.6766e-02	–	7.2118e-04	–	3.3840e-01	–
5.0000e-02	3.5456e-08	5.53	1.4338e-02	1.71	1.7620e-04	2.03	2.1567e-01	0.65
2.5000e-02	3.1101e-10	6.83	3.8738e-03	1.89	4.2802e-05	2.04	1.1837e-01	0.87
1.2500e-02	1.6178e-12	7.59	9.9179e-04	1.97	1.0794e-05	1.99	7.3826e-02	0.68
6.2500e-03	9.3259e-15	7.44	2.4982e-04	1.99	2.8216e-06	1.94	3.7448e-02	0.98
3.1250e-03	4.4409e-15	**	6.2612e-05	2.00	7.3195e-07	1.95	1.4685e-02	1.35
1.5625e-03	4.4409e-15	**	1.5663e-05	2.00	1.8490e-07	1.99	4.6908e-03	1.65
7.8125e-04	5.7732e-15	**	3.9163e-06	2.00	4.6297e-08	2.00	1.2625e-03	1.89

Table 5: $k = s = 2$.

h	H-error	rate	M_1-error	M_2-error	solution error	rate
1.0000e-01	5.0415e-03	–	5.3291e-15	1.6653e-16	1.2173e-01	–
5.0000e-02	9.2412e-04	2.45	3.5527e-15	2.4980e-16	5.0456e-02	1.27
2.5000e-02	6.3056e-05	3.87	4.4409e-15	6.9389e-17	1.7528e-02	1.53
1.2500e-02	4.3554e-06	3.86	4.8850e-15	5.5511e-17	3.2850e-03	2.42
6.2500e-03	2.7750e-07	3.97	5.3291e-15	1.6653e-16	4.9393e-04	2.73
3.1250e-03	1.7396e-08	4.00	1.2879e-14	8.3267e-17	4.3386e-05	3.51
1.5625e-03	1.0880e-09	4.00	1.0658e-14	9.7145e-17	2.8164e-06	3.95
7.8125e-04	6.8009e-11	4.00	1.1546e-14	1.6653e-16	1.7802e-07	3.98

Table 6: $k = 4, s = 2$ (n.c. means non convergence of the nonlinear iteration).

h	H-error	rate	M_1-error	rate	M_2-error	rate	solution error	rate
1.0000e-01	n.c.	–	n.c.	–	n.c.	–	n.c.	–
5.0000e-02	6.2703e-07	–	9.3456e-05	–	3.4242e-06	–	5.0766e-02	–
2.5000e-02	2.9231e-09	7.75	5.9252e-06	3.98	3.7482e-07	3.19	1.7521e-02	1.53
1.2500e-02	1.2728e-11	7.84	3.8789e-07	3.93	2.7360e-08	3.78	3.2841e-03	2.42
6.2500e-03	4.8406e-14	8.04	2.4439e-08	3.99	1.7773e-09	3.94	4.9391e-04	2.73
3.1250e-03	5.7732e-15	**	1.5298e-09	4.00	1.1215e-10	3.99	4.3387e-05	3.51
1.5625e-03	6.2172e-15	**	9.5647e-11	4.00	7.0264e-12	4.00	2.8167e-06	3.95
7.8125e-04	1.0658e-14	**	5.9779e-12	4.00	4.3947e-13	4.00	1.7804e-07	3.98

Table 7: Mean number of blended iterations (38) per step.

h	$s = 1$				$s = 2$	
	$k = 1$	$k = 2$	$k = 3$	$k = 4$	$k = 2$	$k = 4$
1.0000e-01	8.7	9.1	9.2	9.2	16.6	−
5.0000e-02	6.3	6.4	6.4	6.5	16.1	16.1
2.5000e-02	5.5	5.6	5.6	5.7	15.0	15.0
1.2500e-02	4.8	4.9	4.9	4.9	13.0	13.0
6.2500e-03	4.4	4.5	4.5	4.6	11.0	11.0
3.1250e-03	4.3	4.3	4.3	4.3	9.0	9.0
1.5625e-03	4.1	4.1	4.2	4.2	7.0	8.0
7.8125e-04	3.7	3.9	3.9	3.9	6.0	7.0
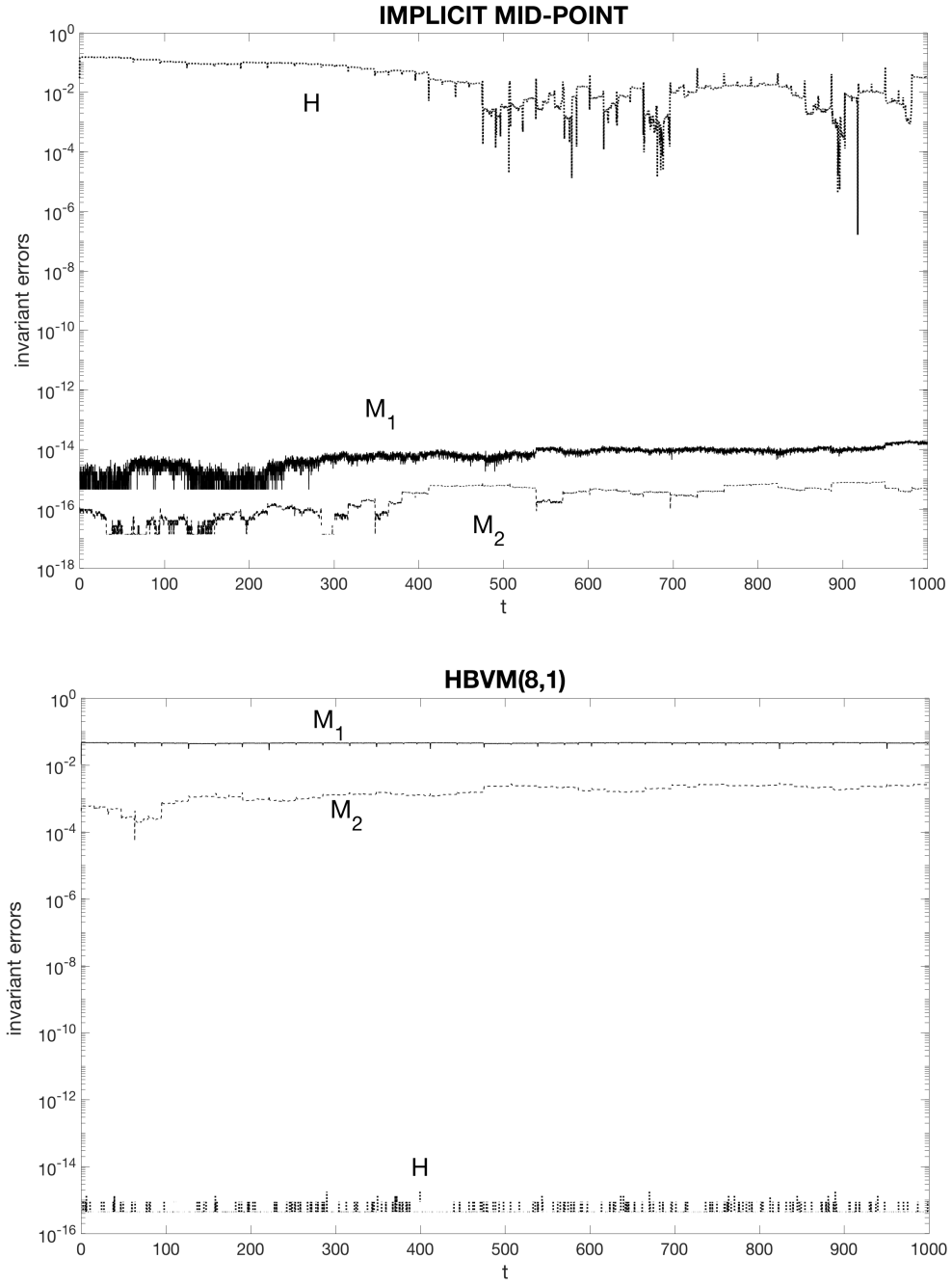
Figure 2: Problem (1)-(39), errors in the numerical invariants (H, M_1, M_2) for the implicit mid-point (upper plot) and the HBVM(8,1) methods, both used with time-step $h = 0.1$.
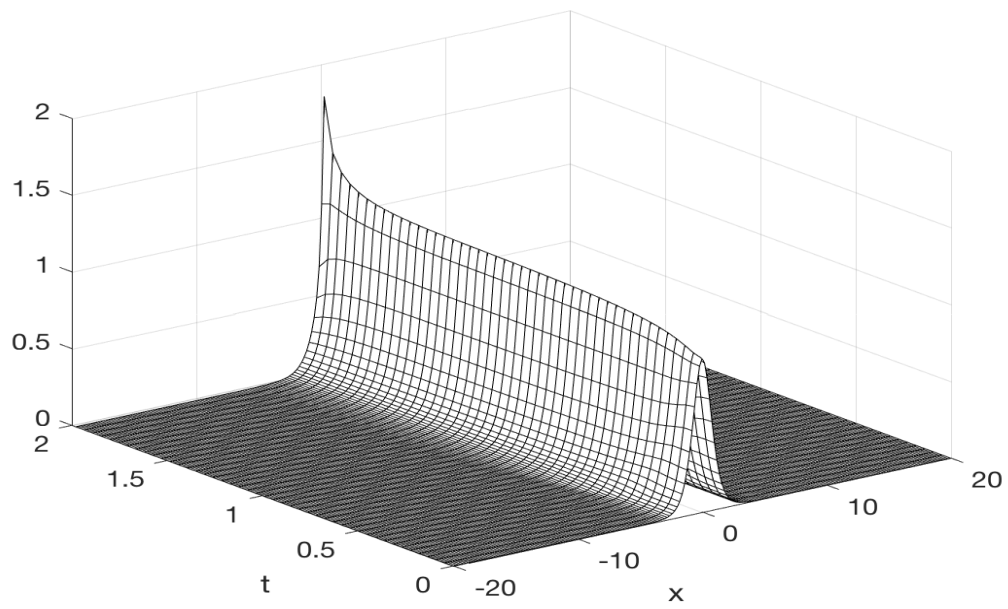
28

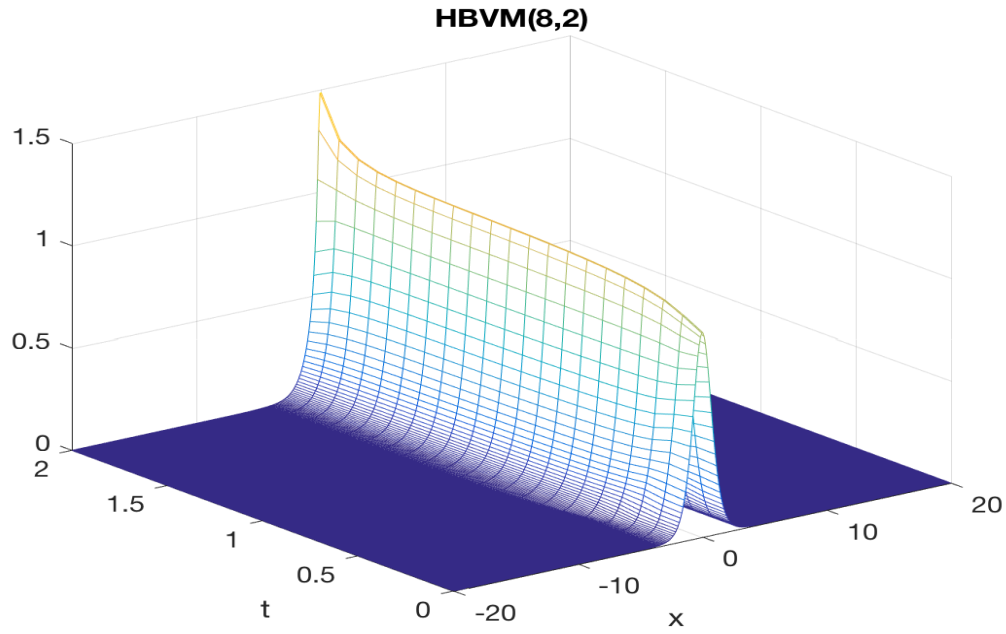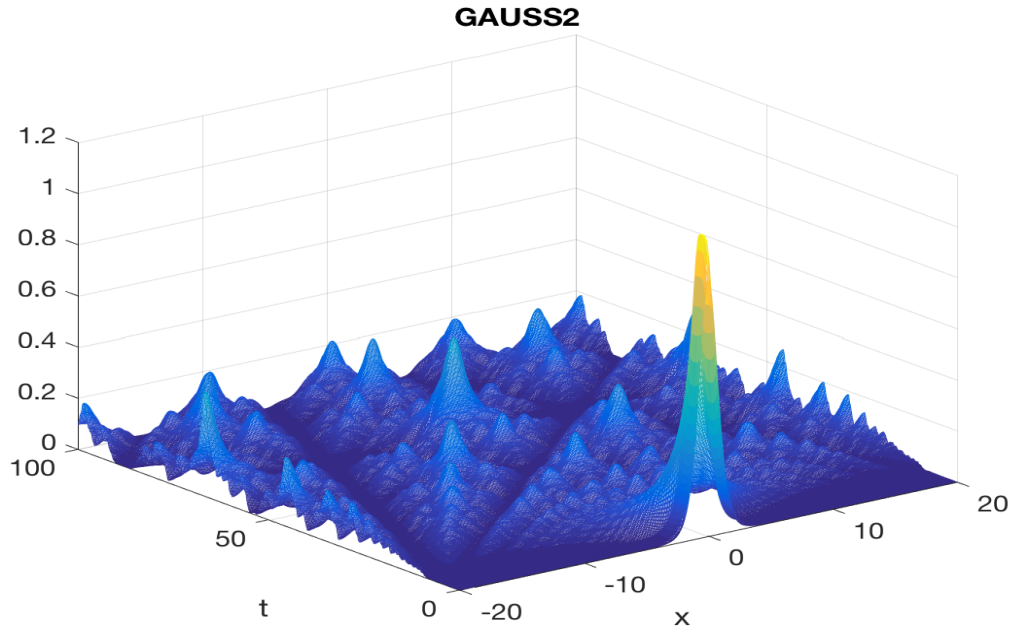Figure 3: Problem (1)-(40), solution blow-up about $t = 2$.

Figure 4: Problem (1)-(40), solution provided by the symplectic 2-stage Gauss method (upper plot) and the energy-conserving HBVM(8,2) method (lower plot) both using the parameters (41).